GHz Rabi Flopping to Rydberg States in Hot Atomic Vapor Cells

B. Huber, T. Baluktsian, M. Schlagmüller, A. Kölle, H. Kübler, R. Löw, and T. Pfau

5. Physikalisches Institut, Universität Stuttgart, Pfaffenwaldring 57, 70550 Stuttgart, Germany
(Received 11 July 2011; published 5 December 2011)

We report on the observation of Rabi oscillations to a Rydberg state on a time scale below 1 ns in thermal rubidium vapor. We use a bandwidth-limited pulsed excitation and observe up to 6 full Rabi cycles within a pulse duration of ∼4 ns. We find good agreement between the experiment and numerical simulations based on a surprisingly simple model. This result shows that fully coherent dynamics with Rydberg states can be achieved even in thermal atomic vapor, thus suggesting small vapor cells as a platform for room-temperature quantum devices. Furthermore, the result implies that previous coherent dynamics in single-atom Rydberg gates can be accelerated by 3 orders of magnitude.

The properties of Rydberg atoms are dominated by very loosely bound electrons moving on large orbits around a charged nucleus. They can easily be a few thousand times larger in size than ground-state atoms. Because of the weak bond, even small electric fields can induce large dipole moments and therefore give rise to strong interactions between Rydberg atoms. This, in turn, leads to strong optical nonlinearities and collective quantum behavior in a frozen ensemble of atoms as, e.g., the excitation blockade into Rydberg states [1–3]. These strong interactions are the basis for various applications of Rydberg atoms in quantum information processing [4–6] and sensing [7]. Most recently, two seminal experiments demonstrated with the help of the Rydberg blockade first gate operations between two individually trapped ultracold atoms [8,9]. In these experiments, the bandwidth of the coherent optical excitation rate, and by this the time of the gate operation, has been limited to the MHz scale. The limit is mainly due to the small spatial overlap between low-lying electronic states and the extended Rydberg states and due to the usage of medium-power cw laser systems. It is of fundamental importance to increase the speed of the coherent excitation to allow for more complex algorithms during the limited time set by decoherence processes. One way to overcome this technical limitation is the use of coherent, i.e., bandwidth-limited pulsed laser systems for the excitation. We show that Rabi cycles to Rydberg states below 1 ns are feasible, resulting in a speedup by 3 orders of magnitude.

For such short evolution times, even atoms at room temperature can be used to observe Rabi flopping to Rydberg states, as they can be considered frozen on this time scale. This opens up new horizons for room-temperature quantum devices based on the ensemble Rydberg blockade which have been described in various proposals [6,7,10,11]. First steps towards the fabrication of microscopic vapor cells have already been accomplished [12,13]. Standard technologies in the production process of these cells will allow for full integration of larger cell arrays [14] and applications, e.g., for linear quantum

computing [15], are in reach. From previous work on electromagnetically induced transparency in thermal vapor involving Rydberg states, a coherence time limit of a few 10 nanoseconds can be inferred [16,17], which is due to transient broadening and wall interactions.

In this Letter, we report on the observation of Rabi oscillations to a Rydberg state in hot atomic vapor. We accomplish this by driving the dynamics fast compared to any decoherence processes. We achieve Rabi cycle times of ∼500 ps, resulting in a coherent phase evolution of up to 12π which is limited only by the length of the pulse used in the experiment. In the following, we first briefly describe the experimental setup and measuring scheme we used to obtain the oscillation data, which is presented subsequently. The behavior of the oscillations for different driving intensities and laser detunings is shown. We give qualitative arguments for the behavior and compare with numerical simulations based on a very simple model.

For the following experiments, we use a 5 mm glass cell containing rubidium vapor at $T \sim 130\,°C$ with the two stable isotopes occurring at natural abundance (^{85}Rb: 72.2% and ^{87}Rb: 27.8%). The atomic density was determined by absorption spectroscopy to be 7.4×10^{12} cm^{-3}. We address the Rydberg state in ^{85}Rb using a two-photon transition via an intermediate state. The excitation scheme is $5S_{1/2} \rightarrow 5P_{3/2} \rightarrow 30S_{1/2}$, denoted by $|1\rangle$, $|2\rangle$, and $|3\rangle$ in the following [Fig. 1(a)]. The ground-state transition is driven by a cw laser at ∼780 nm. This laser is locked to the center of the Doppler valley of the ^{85}Rb, $5S_{1/2}$, $F = 2 \rightarrow 5P_{3/2}$ transition in order to ensure a large spectral distance from any other ground-state transition (from either isotope). For the upper transition to the Rydberg state, a bandwidth-limited laser pulse at ∼480 nm is employed. The pulse is created with a seeded dye amplifier in four-pass configuration similar to the one described in [18]. The temporal shape of the pulse is roughly Gaussian with a full width of ∼2.5 ns at half maximum [Fig. 1(b), lower half]. The corresponding Rabi frequencies are $\Omega \sim 2\pi \times 220$ MHz for the cw light
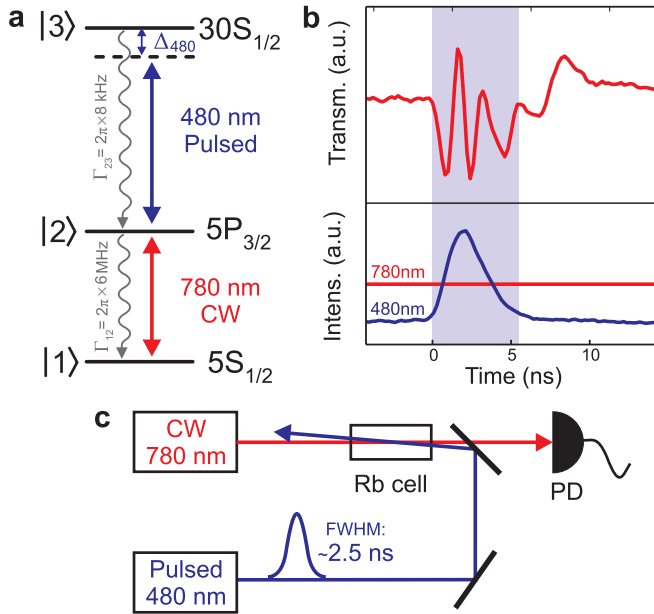
FIG. 1 (color online). Schema of the experiment. (a) The Rydberg state is addressed with a two-photon transition via an intermediate state. The laser for the upper transition is pulsed. (b) Transmission signal of the 780 nm laser (upper half) and corresponding laser intensities (lower half) as a function of time. (c) Simplified schematic of the optical setup.

and $\Omega_{480,\text{peak}} \sim 2\pi \times 2.2$ GHz for the maximum peak Rabi frequency of the pulse [19]. Note that all Rabi frequencies are much larger than the decay rate of any state involved such that the dynamics is not dominated by decay on the relevant time scales. The two laser beams are overlapped in the vapor cell in almost counter-propagating ($\theta = 171.5°$) configuration [Fig. 1(c)]. We observe the transmission of the 780 nm laser with a fast photodetector, thus probing the coherence between the lower two levels. In order to avoid averaging over different Rabi frequencies, we ensure that only light from a homogeneously illuminated region of the cell is detected. We achieve this by selecting an almost homogeneous intensity distribution in the blue beam profile with a circular pinhole and imaging it into the cell via 1:1 imaging. We then cut out a part of the illuminated volume by use of another 1:1 imaging onto a second pinhole which resides directly in front of the photodetector. This way, we detect a homogeneously illuminated region also with respect to the 780 nm laser. This region contains about 3×10^8 atoms.

Both lasers are linearly polarized in the same direction. Note that, due to the large bandwidth of the excitation dynamics, the hyperfine structure in the $5P_{3/2}$ and the $30S_{1/2}$ state is not resolved while it is resolved in the $5S_{1/2}$ ground state. This means that the typical inhomogeneous distribution of matrix elements in narrow band experiments [20] (e.g., in the MHz range as in cold atom experiments) is not present here, and the medium reduces in good approximation to a thermal ensemble of driven

three-level atoms despite the initial mixture of hyperfine ground states.

A typical transmission curve we observe (averaged over 5 curves) is plotted in the upper half of Fig. 1(b). Before the pulse, the atoms represent an effective two-level system (not taking into account the second hyperfine ground state) and are in a steady state together with the strongly driving 780 nm light. During the time of the pulse (depicted by the shaded area), oscillations in the transmission appear. For a resonant pulse, these oscillations mainly correspond to Rabi flopping between the intermediate and the Rydberg state. Depending on the phase of the oscillation at the end of the pulse, a certain fraction of the occupation remains in the Rydberg state. Further oscillatory behavior in the time after the pulse originates from Rabi oscillations between the lower two states, as the remaining two-level system is not in equilibrium immediately after the pulse. Those oscillations decay quickly, and the system returns into a steady state.

We studied the behavior of the system for different pulsed laser intensities [Fig. 2(a)]. With both lasers on resonance, we recorded transmission curves for pulsed laser peak intensities from $I_{480,\text{peak}} = 0\text{--}21$ MW/cm^2. With the corresponding dipole matrix element (taken from [6]), this translates to Rabi frequencies of $\Omega_{480,\text{peak}} \sim 2\pi \times (0\text{--}2.3)$ GHz. Each time trace in the figure is an average of 5 transmission curves. For a three-level system in ladder configuration with both transitions resonantly driven, one expects the eigenfrequencies to behave like $\Omega_{\text{eff,res}} \propto \sqrt{\Omega_{780}^2 + \Omega_{480}^2}$. Indeed, points of constant phase exhibit this square-root-like behavior as a function of pulse intensity.

We have done numerical simulations of a three-level system with a density matrix approach using the Liouville–von Neumann equation [21]

$$\frac{\partial \hat{\rho}}{\partial t} = -\frac{i}{\hbar}[\hat{H}, \hat{\rho}] + \hat{L}(\hat{\rho}),$$

with the Hamiltonian in the rotating wave approximation

$$\hat{H} = \hbar \begin{pmatrix} 0 & \frac{1}{2}\Omega_{780} & 0 \\ \frac{1}{2}\Omega_{780}^* & -\Delta_{780} & \frac{1}{2}\Omega_{480}(t) \\ 0 & \frac{1}{2}\Omega_{480}^*(t) & -\Delta_{780} - \Delta_{480} \end{pmatrix}$$

and the Liouville operator

$$\hat{L}(\hat{\rho}) = \Gamma_{12} \begin{pmatrix} \rho_{22} & -\frac{1}{2}\rho_{12} & 0 \\ -\frac{1}{2}\rho_{21} & -\rho_{22} & -\frac{1}{2}\rho_{23} \\ 0 & -\frac{1}{2}\rho_{32} & 0 \end{pmatrix}$$
$$+ \Gamma_{23} \begin{pmatrix} 0 & 0 & -\frac{1}{2}\rho_{13} \\ 0 & \rho_{33} & -\frac{1}{2}\rho_{23} \\ -\frac{1}{2}\rho_{31} & -\frac{1}{2}\rho_{32} & -\rho_{33} \end{pmatrix}$$
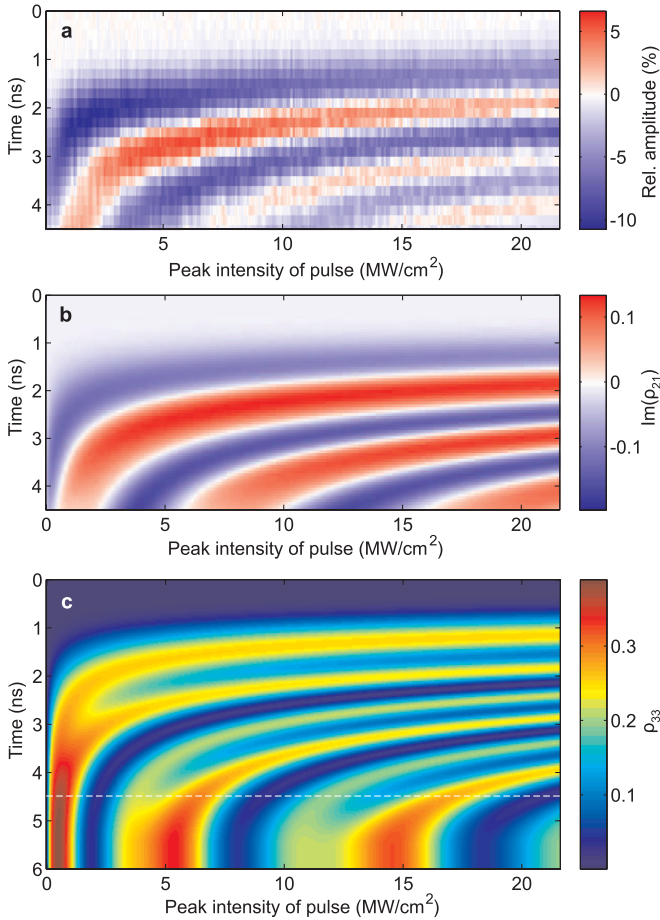
FIG. 2 (color online).   Rabi oscillations for different pulse intensities. (a) Oscillations in the transmission of the 780 nm laser during the pulse. Both lasers are resonant to their respective transitions. The beginning of the pulse is at $t = 0$ ns. (b) A corresponding simulation provides results for $\mathrm{Im}(\rho_{21})$, which is connected to the absorption. The behavior of the experimental data is reproduced in excellent agreement. (c) Simulated Rydberg occupation ρ_{33}. Above the dashed line, the dynamics is dominated by the pulsed laser. All relevant parameters are described in the text.

that includes the decay rates $\Gamma_{12} = 2\pi \times 6$ MHz [22] and $\Gamma_{23} = 2\pi \times 8$ kHz [23]. The initial conditions are given by the steady-state solution ($\partial \hat{\rho}/\partial t = 0$) in the absence of the pulsed laser ($\Omega_{480} = 0$). We account for the thermal distribution of the atoms by solving this equation separately for each velocity class with the respective Doppler detunings and weighting the individual results accordingly. The quantity connected to the absorption is the imaginary part of the coherence of the $|1\rangle \rightarrow |2\rangle$ transition $\mathrm{Im}(\rho_{21})$ [Fig. 2(b)]. For small relative variations, proportionality between the transmission and $\mathrm{Im}(\rho_{21})$ can be assumed. The behavior of $\mathrm{Im}(\rho_{21})$ is found to be in excellent agreement with the experiment.

While our experimental approach does not allow for direct observation of the Rydberg population ρ_{33}, this quantity is accessible in the simulations [Fig. 2(c)]. It can

be seen that the population oscillates at twice the frequency that can be observed in the transmission. This is expected, as the atomic state acquires a phase of π for each round trip $|2\rangle \rightarrow |3\rangle \rightarrow |2\rangle$. In contrast to $\mathrm{Im}(\rho_{21})$, ρ_{33} is not sensitive to phases. Therefore, the evolution of $\mathrm{Im}(\rho_{21})$ recurs after two round trips, whereas the evolution of ρ_{33} recurs after one. The data shows that, during the time of the pulse (~ 4 ns), we achieved to drive Rabi cycles with a phase of up to 12π.

After the pulse, the Rydberg population stays nearly constant due to the long lifetime of the Rydberg state. The lifetime is limited by Rydberg–ground-state collisions and transient broadening which not included in the simulations but expected to be on the order of a few MHz [24]. By adjusting the pulse intensity, the phase of the oscillation at the end of the pulse can be chosen conveniently such that a maximum Rydberg population remains after the pulse. For our experimental parameters, where the experiment was not optimized for high Rydberg population, we can infer that $\rho_{33} \sim 35\%$. This is, besides thermal velocity distribution, due to the fact that we start with a steady state, where the intermediate state population is $\sim 50\%$. With a sequence, however, where also the lower transition is addressed by a pulse, the limit of 50% does not apply anymore. Impromptu simulations of simultaneous pulses for both transitions with Rabi frequencies in the GHz range show that, for pulse lengths of $\lesssim 1$ ns, Rydberg occupations of over 90% can easily be achieved.

Furthermore, we investigated the dependence of the system on the detuning of the pulsed laser. For these measurements, we used a peak pulse intensity of 21 MW/cm^2. The oscillations observed in the transmitted beam [Fig. 3(a)] are reproduced in very good agreement by simulations [Fig. 3(b)]. It can be seen that the oscillations become slower with increasing detuning. This behavior may seem counterintuitive at first glance, as Rabi oscillations in a two-level system scale like $\Omega_{\mathrm{eff}} \propto \sqrt{\Omega^2 + \Delta^2}$ and thus get faster with detuning. In our system, however, the laser pulse induces a dynamic Autler-Townes splitting between the states $|2\rangle$ and $|3\rangle$. Two oscillatory modes occur, one arising from each of the split lines [25]. For an atom at rest [Fig. 3(c)], the two modes (indicated by the black lines of positive and negative slope, respectively) are symmetric and the highest oscillation amplitude can be found for zero pulse detuning. For increasing pulse detuning, one of the split lines approaches the resonance. The corresponding mode therefore becomes slower (solid parts of the lines), while the other mode becomes faster (dashed parts of the lines). For atoms with a finite velocity, however, both lasers appear Doppler-shifted such that resonance to one of the split lines can actually be reached for a certain pulse detuning. Hence, the slower mode becomes more intense as the pulse detuning approaches this resonance. At the same time, the faster mode becomes more faint. Additionally, the visibility of the faster mode is
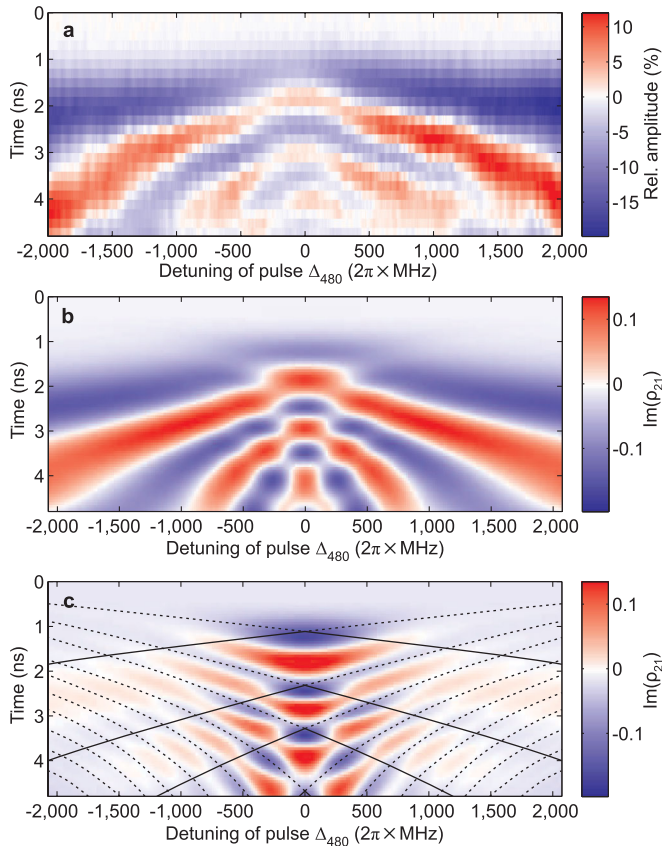
FIG. 3 (color online). Rabi oscillations for different detunings of the pulse. (a) Oscillations in the transmission of the 780 nm laser during the pulse. This laser is resonant to the $|1\rangle \rightarrow |2\rangle$ transition. The beginning of the pulse is at $t = 0$ ns. (b) Simulation of $\mathrm{Im}(\rho_{21})$ which is connected to the absorption. The behavior agrees very well with the experimental data. (c) Simulated behavior of $\mathrm{Im}(\rho_{21})$ for the velocity class $v = 0$ only. The black lines (both dashed and solid) indicate points of constant phase for the two oscillatory modes that occur.

reduced further by the fact that the coupling is varying in time due to the envelope of the pulse. Averaging over all velocity classes then yields the observed behavior [Figs. 3(a) and 3(b)].

In summary, we have found that the observed GHz Rabi oscillations to a Rydberg state in thermal vapor show a perfect match with a very simple theoretical model based on three levels only. This is surprising at first sight, as rubidium has a complex hyperfine structure. However, the large bandwidth of the fast excitation greatly simplifies the situation, as compared to slow dynamics, which suffers from a state-dependent inhomogeneous distribution of coupling strengths to the light field. This reduces the necessity for initialization of ensembles in quantum devices. It also simplifies the physics of the Rydberg blockade. In future experiments, we therefore intend to use the observation of coherent dynamics to demonstrate the Rydberg blockade and the characteristic $\sqrt{N}$ scaling

of the collective Rabi frequency in thermal vapor, as has been done in ultracold ensembles previously [26–28]. We envisage the application of coherent dynamics in Rydberg-blockaded thermal ensembles in the realization of single-photon emitters [11] and absorbers [7].

[1] D. Tong *et al.*, Phys. Rev. Lett. **93**, 063001 (2004).
[2] K. Singer *et al.*, Phys. Rev. Lett. **93**, 163001 (2004).
[3] T. Vogt *et al.*, Phys. Rev. Lett. **97**, 083003 (2006).
[4] D. Jaksch *et al.*, Phys. Rev. Lett. **85**, 2208 (2000).
[5] M. D. Lukin *et al.*, Phys. Rev. Lett. **87**, 037901 (2001).
[6] M. Saffman, T. Walker, and K. Mølmer, Rev. Mod. Phys. **82**, 2313 (2010).
[7] J. Honer *et al.*, Phys. Rev. Lett. **107**, 093601 (2011).
[8] L. Isenhower *et al.*, Phys. Rev. Lett. **104**, 010503 (2010).
[9] T. Wilk *et al.*, Phys. Rev. Lett. **104**, 010502 (2010).
[10] R. Löw and T. Pfau, Nat. Photon. **3**, 197 (2009).
[11] M. Saffman and T. G. Walker, Phys. Rev. A **66**, 065403 (2002).
[12] T. Baluktsian *et al.*, Opt. Lett. **35**, 1950 (2010).
[13] D. Sarkisyan *et al.*, Opt. Commun. **200**, 201 (2001).
[14] W. Yang *et al.*, Nat. Photon. **1**, 331 (2007).
[15] A. Politi *et al.*, Science **320**, 646 (2008).
[16] A. K. Mohapatra, T. R. Jackson, and C. S. Adams, Phys. Rev. Lett. **98**, 113003 (2007).
[17] H. Kübler *et al.*, Nat. Photon. **4**, 112 (2010).
[18] A. Schwettmann *et al.*, Appl. Opt. **46**, 1310 (2007).
[19] Rabi frequencies extracted from the best fit of simulations to the data. $\Omega_{480,\mathrm{peak}}$ agrees within 5% with the value deduced from the peak intensity of the pulse.
[20] M. Reetz-Lamour *et al.*, Phys. Rev. Lett. **100**, 253001 (2008).
[21] M. Fleischhauer, A. Imamoglu, and J. Marangos, Rev. Mod. Phys. **77**, 633 (2005).
[22] U. Volz and H. Schmoranzer, Phys. Scr. **T65**, 48 (1996).
[23] D. B. Branden *et al.*, J. Phys. B **43**, 015002 (2010).
[24] D. C. Thompson *et al.*, Phys. Rev. A **35**, 690 (1987).
[25] K. Rzążewski and M. Florjánczyk, J. Phys. B **17**, L509 (1984).
[26] R. Heidemann *et al.*, Phys. Rev. Lett. **99**, 163601 (2007).
[27] E. Urban *et al.*, Nature Phys. **5**, 110 (2009).
[28] J. D. Pritchard *et al.*, Phys. Rev. Lett. **105**, 193603 (2010).